VISIBILITY ASPECTS OF PASSIVE AND ACTIVE OPTICAL MONITORING OF SPACE DEBRIS IN LOW EARTH ORBITS

J. Radtke[a,b], I. Buske[a], U. Voelker[a], F. Friederich[a]
[a]Institute of Technical Physics, German Aerospace Center (DLR),
Pfaffenwaldring 38-40, 70569 Stuttgart
Germany
[b]Institute of Aerospace Systems, TU Braunschweig,
Hermann-Blenk-Str. 23, 38108 Braunschweig
Germany

Overview

Optical observation of orbital objects using passive reflection of sun light is a well-known technique to characterize the space debris population in GEO. Robotic telescopes are scanning every night under automated operation the GEO zone to identify non-catalogued objects. The accuracy is determined by the GPS controlled exposure time.
Active satellite laser ranging (SLR) methods, on the other hand, are used to measure distances to LEO and MEO satellites with accuracy down to a few millimeters. However, SLR system operators have access to accurate orbit predictions. This accuracy is much better than the “Two Line Elements” (TLE) orbit predictions which are open for public access.
Both methods are combined in a concept proposed by DLR Institute of Technical Physics to detect and track space debris in LEO. As a part of this concept visibility analyses were performed for passive space debris monitoring during twilight conditions and photon budgets are estimated for active laser ranging. The investigations are done by taken into account an existing observation telescope. Furthermore, the results of ranging campaigns performed in cooperation with the SLR station in Graz confirmed our conceptual SLR requirements of a future fully functional space debris monitoring system. Different dependencies are reviewed especially the visibility of different object sizes in relation to their orbit altitude under passive and active illumination.

1. INTRODUCTION

Currently, the Institute of Technical Physics at the DLR in Stuttgart is building a test station for passive optical acquisition of space debris at the Schwäbische Sternwarte in Stuttgart Uhlandshöhe[1]. Several studies have been performed to estimate the performance of this station beforehand. These studies are both performed analytically and with the help of PROOF2009 simulations. Recent results of ranging campaigns performed in cooperation with the SLR station in Graz confirmed our conceptual SLR requirements of a future fully functional space debris monitoring system and will be published this year.

In this paper, an overview of the test station at Uhlandshöhe Stuttgart is presented and its expected performance is investigated.

2. THE TEST STATION

At first, the test station at Stuttgart is described briefly. As this station is currently under construction, all the described hardware is already available for the station.

2.1. Telescope

As telescope, the PlaneWave CDK 17 telescope was chosen. This telescope is a corrected Dall-Kirkham telescope type. A big advantage of these is the near diffraction limited spot size and coma free image available over a large field plane. A focal ratio up to f/4.49 provides a large field of view at reasonable costs. The basic characteristics of the telescope are given in TAB 1, both for the standard setting as well as for a setting with a focal reducer. This reducer can be used to reduce the focal length of the telescope, and by this enlarge the field of view to detect more objects during an observation period.

	normal	w/ focal reducer
aperture	432 mm	
aentral obstruction	39 %	
focal length [mm]	2939	1939.68
focal ratio	f/6.8	f/4.49
spot size [µm]	6.5	7.3
focal plane (diameter, [mm])	52	

TAB 1: Characteristics of CDK 17 telescope (Plane Wave Instruments, 2012).

[1] www.sternwarte.de

2.2. Cameras

As cameras, two different kinds were chosen to be used at the test station: A high sensitive EMCCD camera, the ANDOR DU 897 ultra, and one standard astronomy camera, the FLI PL 16803. Basic characteristics of these cameras are given in TAB 2. Reasons for the choice of these cameras are given in section 2.2.1. The values stated in brackets are valid for the use with the focal reducer.

	Andor	FLI PL	perfect
field of view [°]	0.16 (0.24)	0.7 (1.09)	0.78 (1.18)
pixels per row	512	4096	2500
pixel size [µm]	16	9	16
pixel scale [arcsec/pix]	1.123 (1.702)	0.632 (0.957)	1.124 (1.702)
exposure time [s]	> 0.01	> 0.02	> 0.01

TAB 2: Basic camera data.

2.2.1. SNR of low light imaging cameras

To apply the best technology available for sun illuminated space debris imaging under very low light conditions one can choose between different scientific focal plane arrays. The main requirement is that the camera shall be able to detect signal photons and distinguish them from the background and noise level. Most astronomical cameras have been developed for long exposure times. High resolution images (>16 mega pixel) and the suppression of read out noise causes typical long read out time. Due to this, most of these cameras are not suitable for our application. As we are dealing with short exposure times, dark noise can be also assumed to be negligible.
Recent developments in CCD and CMOS technology have improved the sensor sensitivity. New enhancements for scientific (s)CMOS sensors greatly reduced the read out noise to < 2.5 e-/pixel which is the main source of noise in fast read out camera systems. Efforts are taken to improve the quantum efficiency to >60%. Advantages of the sCMOS technology are the large (5 mega pixel) and sensitive pixel area. Thereby local regions of interest can be readout with frame rates of several kHz.

Former used low noise interline CCD are combined with an inherent gain register to amplify the photoelectrons prior to the read out circuit. This electron multiplication (EM)CCD offers single photon detection. The outstanding effective signal-to-noise ratio can be suppressed below 1 e-/pixel. Associated with this amplification process some additional noise with a typical factor of 2 is created. That is why the optimal regime for EMCCD sensors is found for very low photon fluxes combined with high frame rates. The additional noise factor can also be interpreted as a QE loss compared to sCMOS and interline CCDs. The original QE of >90% will be reduced to an equivalent QE of nearly 45%.

With our decision to choose the EMCCD Andor Ultra we have the chance to detect very faint space debris objects moving fast around the earth in low orbits. New developments are under progress to increase the small chip size of EMCCDs.

Additionally, for wide field and high spatial resolution application a front illuminated FLI interline CCD camera will be used. Due to camera cooling, which decreases the dark current, low noise and long exposure images will be also available.

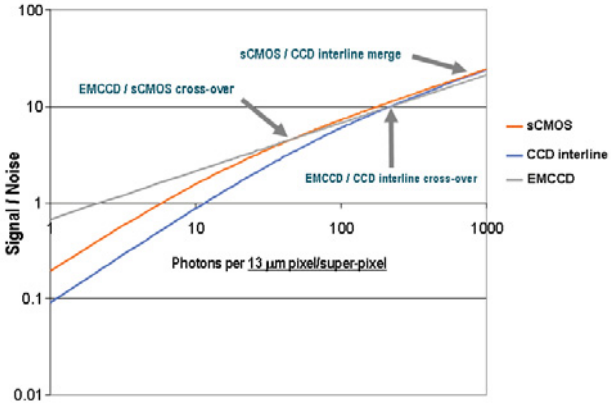

Figure 1: SNR of different focal arrays technologies.

Figure 1 shows the signal-to-noise ratio (SNR) characteristics of interline CCD, EMCCD and sCMOS. To compare the different technologies the SNR is scaled to the same pixel size using binned pixel for sCMOS and interline CCD. It is clearly shown that there is a trade-off between the technologies. EMCCD are preferred in the case of a receiving photon flux below 20 photons/pixel. Otherwise sCMOS and interline CCD are favored. (Coates, Fowler, & Holst, 2009)

3. PROOF2009

Several analyses have been performed using the software PROOF2009[2]. To put the results in context, a brief introduction about PROOF2009 shall be given. For a more comprehensive insight into the functionality of the software, please refer to (Gelhaus, Flegel, & Wiedemann, 2011).

3.1. General

PROOF2009 (*P*rogram for *R*adar and *O*ptical *F*orecasting with reference epochs till May 2009) has been developed at the Institute of Aerospace Systems of the TU Braunschweig under ESA contract. The software can be used for three purposes:

- Validation of space debris models,
- Analysis of measurement data,
- Planning of observation campaigns,

To conduct a simulation, several modes are available. These include statistical, deterministic or hybrid modes, both for radar and optical wavelengths. Also, it can be chosen if the sensor is ground or space based, if it shall track objects and if the observation is mono- or bistatic (for radars). As for the present paper only ground-based staring observations with an optical telescope are of interest, all further information refer to this mode.

[2] Software available via www.master-model.de

Furthermore, only statistical simulations have been performed.

3.2. Considered effects and inputs

In this passage, a short overview of the considered effects and the assumptions made in PROOF2009 shall be given.

3.2.1. Background radiation

The model for the background radiation is described in (Daniels, 1977). It has to be noted that this model only considers natural sources for the background radiation. So no artificial sources like the glow of cities are considered in PROOF at any point.
The sources can be split-up into two groups: First the discrete sources, which contain the sun, the moon, bright stars up to a chosen magnitude and the planets. When the sun is above the horizon, or the moon in the field of view, PROOF assumes no detection to be possible. All other sources (these are faint stars, zodiacal light, airglow, galaxies and atmospherically scattered light from all sources, including sun during twilight and the moon) are considered to be continuous. This continuous source is modeled over the night sky and fitted to the actual line of sight.

3.2.2. Atmospheric influences

The atmospheric influence on the received signal from an orbiting object is taken into account by the atmospheric transmission. It is considered to be wavelength dependent. This dependency can be changed in a file to adjust it to the site's conditions. Furthermore, a change of the transmission regarding the actual elevation of the line of sight is included.
The effect of refraction is only realized for deterministic simulations, atmospheric turbulences are not implied at all. For the irradiation of objects by the sun, no atmospheric effects are considered. This seems fair enough, as there would be an effect only on very some very low orbiting objects which would be affected by this.

3.2.3. Objects

The objects included in PROOF 2009 are grouped into the most common sources of space debris. These sources are TLE-objects, fragments, sodium-potassium droplets (NaK-droplets), solid rocket motor slag (SRM) and dust, Westford needles and multi-layer insulation (MLI). For each of these object groups, the user can define an albedo within a certain range of standard deviation. Furthermore, these objects are modeled either as spheres or averaged randomly tumbling plates. All objects are modeled as grey bodies. For the statistical mode, space population files referring to ESA's MASTER2009 model are available.

3.2.4. Sensor

The sensor is always assumed to be a square CCD, no overexposure is possible. The telescope itself is working in the range of visible light. Quantum efficiency both from the chip, as well as from the whole optical system can be considered via an input file.

4. PERFORMED VISIBILITY STUDIES

To assess the possible detection of objects, and the range of these detections regarding times, visibility, number of objects etc., several simulations haven been performed with PROOF2009, which results are presented.

4.1. General Inputs

All simulations have been performed with the same base settings. It has been chosen to run statistical analyses with a ground based telescope at Stuttgart Uhlandshöhe. As reference day, the 1st of May has been chosen. For this day, the newest MASTER population time is available and thus propagation times during processing can be avoided. When simulations at additional times have been performed, it is noted in the text. Furthermore, the resolution of the single objects has been enabled. This means that PROOF is taking the statistical data provided by MASTER and re-sampling it to a deterministic amount of particles. This is helping a lot when analyzing the results, as every sighting can be matched to a certain particle. Furthermore, all runs have been performed with 15 Monte Carlo runs, to smoothen statistical artifacts. The simulations have been performed using the hardware described in section 2. Furthermore, as a reference, a perfect camera has been simulated. This camera is assumed to produce no read-out and dark noise, as well as the read out time for the single images is assumed to be zero.

4.2. Integration times

While most of the simulation inputs are already defined by the hardware of the test station, the integration time of the cameras has to be chosen. Optimum would be to integrate always only as long as the object is over one pixel. During further exposure time, only noise from background and other sources is collected. The driving factor for the time one particle needs to pass over one pixel is the angular velocity with which the object is moving. To evaluate these values analytical calculations are done to estimate the flyby pixel exposure time in a first approximation. Assuming a circular orbit in 1000 km over ground the orbital period was determined by means of Kepler's laws. Afterwards the angular velocity related to the observer's point of view was calculated. The telescope is fixed in starring mode. In Figure 2 the angular velocity of a typical LEO debris object passing through the observer's local zenith is shown. With total flyby duration of 1056 s, the angular velocity started at horizon with 200 arcsec/s and reached its maximum value at zenith with 1500 arcsec/s. At lower elevations this maximum will be decreased.

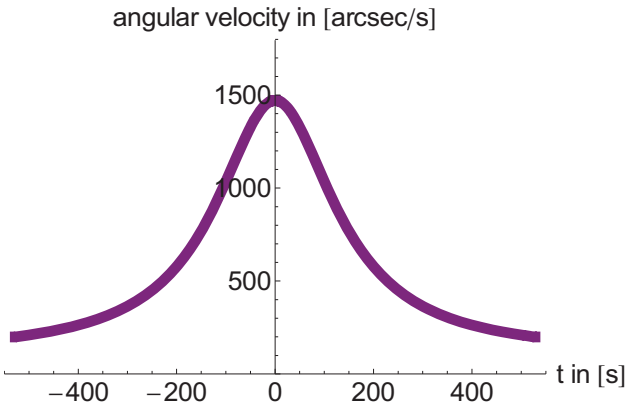

Figure 2: Angular velocity of an LEO object in an altitude of 1000 km on a zenith pass during the flyover.

Taking into account the telescope's focal length (f/6.8: f = 2936 mm; f/4.49: f = 1939 mm) and the camera pixel size one can calculate the field of view per pixel. Andor Ultra features 1.123 arcsec/pixel for f/6.8 and 1.65 arcsec/pixel for f/4.49. While FLI cam is characterized by 0.61 arcsec/pixel for f/6.8 and 0.924 arcsec/pixel for f/4.49. Assuming that the space debris objects can be described as a point source and that the telescope (diffraction limited) spot is smaller than a pixel, the reflected sun light can be collected on only one single pixel. As pointed out in TAB 2 this is the case for the FLI camera. It follows from the above that the maximal exposure time per pixel depends on the angular velocity. In Figure 3 the derived maximum exposure times during flyover are shown. Applying longer exposure times will result in additional background noise floor. Depending on the background light intensity the SNR can be decreased significantly.

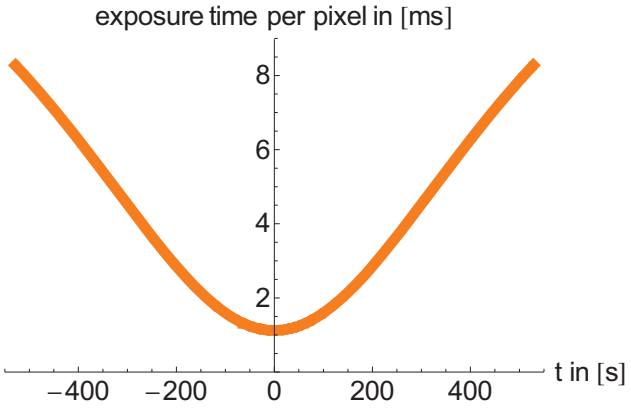

Figure 3: Maximum exposure time of one pixel during flyover of a LEO object.

Another hardware limit has to be proved. Cameras typically provide only a minimal exposure time. Often the minimal exposure time is not restricted by the focal plane array but by the mechanical shutter delay. Therefore the FLI camera is limited by their mechanical shutter opening and closing process to 20 ms. Andor Ultra camera can be exposed down to 10 ms. Compared with the results of PROOF and the analytical calculations this is the limiting parameter.

4.3. Results

4.3.1. Minimum particle size

The first point of interest is the minimum particle size that can be detected. For this, simulations of one night with all three cameras, Andor, FLI PL and Perfect, have been performed. The inputs were set as prior described in section 2. Additionally, integration times of one second have been used, to proof the use of minimal integration times. Furthermore, all simulations have been performed during several times. In here, the results for the reference day are presented. These are shown in Figure 4, Figure 5 and Figure 6. The simulations show the expected result: Due to its high sensitivity, the Andor camera can detect particles down to the near centimeter range. The FLI camera detects objects down to 20 centimeters. Also, due to the low sensitivity, with this camera changing the integration time does not change as much as for the other cameras, with one second integration time, even slightly smaller objects are detected. The perfect camera detects smallest particles, down to sizes of less than one centimeter. As mentioned before, the changing of minimum sizes with the integration time can be explained with a changing SNR. With increasing exposure time (integration), the chip collects much more background and other noises and thus, the SNR decreases. For a better overview, the smallest objects in total are presented in TAB 3.

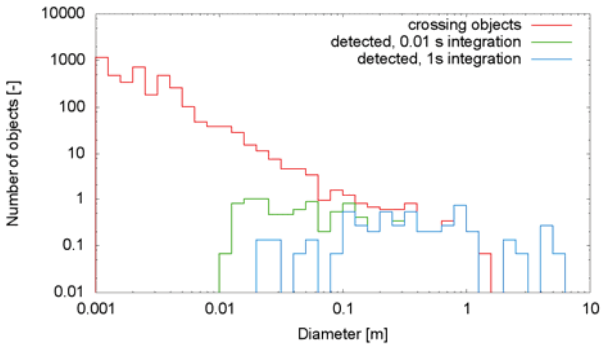

Figure 4: Minimum object size, Andor camera.

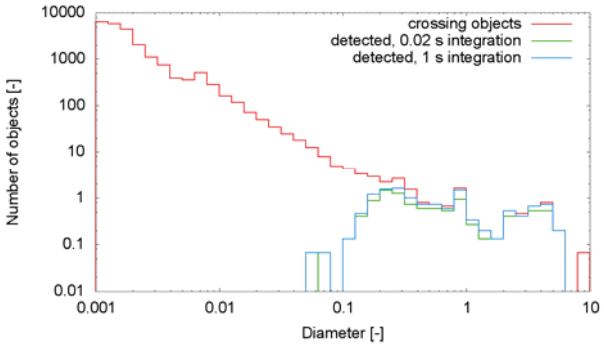

Figure 5: Minimum object size, FLI PL camera.

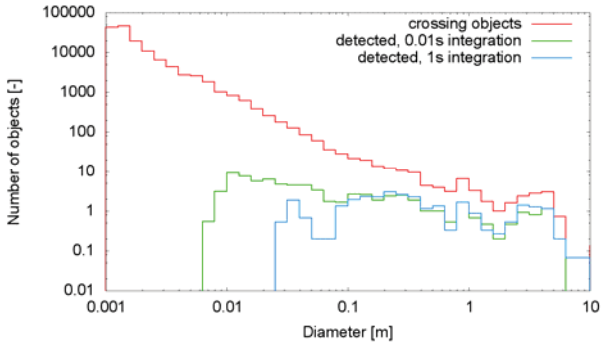

Figure 6: Minimum object size, perfect camera.

camera	minimum object size [m]	/w focal reducer
Andor	0.0187	0.0103
FLI PL	0.216	0.143
Perfect	0.008	0.008

TAB 3: Minimum object sizes.

The same simulations have been performed for the telescope using the focal reducer. By using the reducer, the focal length gets reduced, and thus the field of view enlarged. As seen in here, the sizes of the detected minimum objects basically stay the same. The difference can simply be explained by more objects passing through the field of view, including more detectable small objects. Simulations on further days support this explanation.

4.3.2. Number of particles

Another very important aspect for a Space Debris Surveillance station is the number of particles one can discover passive optically. For this, a large set of simulations has been performed for the Stuttgart site for all cameras under different viewing directions, to find the optimal line of site. As illumination conditions change throughout the year due to the different positions of the sun, these simulations have been performed for all cameras at different times throughout the year, i.e. February, May, August and November. An exemplary result of this is shown in Figure 7. This result shows the mean results of simulations on five different days in the beginning of May 2009. It can be seen that in this time of the year, the maximum number of particles can be detected when looking basically to the East or West directions, which corresponds to elevations of 10° and azimuths of 90° and 270°.

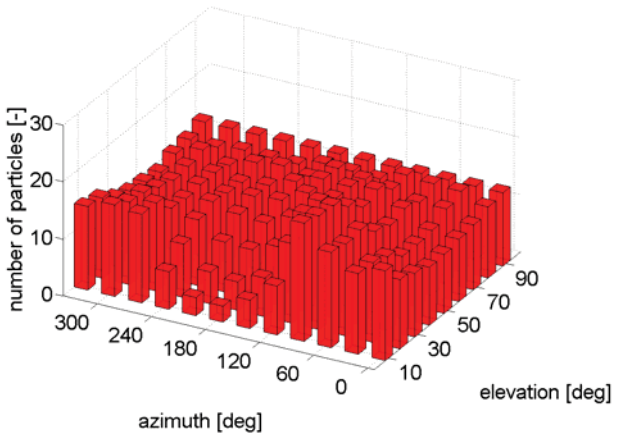

Figure 7: Number of particles per night, beginning May 2009, Andor camera. Peeks are observable for el=10° and az = 90° and az = 270°.

For all cameras, the tendency of the directions is the same, although the total amount of particles is higher for both the FLI and the perfect camera. This is to be explained by the larger field of view. Furthermore, the preferable line of sight changes throughout the year.
In February and December simulations, most particles can be detected when looking directly towards north (el = 10°, az = 0°). In August, the yielded results are similar to the ones from May, just this time looking east is slightly better than looking west. This change of the line of sight can be explained by a combination of the total passing objects, illumination of those and orbit mechanical effects. Most objects pass the field of view when looking at north, the best illumination is reached for azimuths in the southern directions, but changes with the position of the sun over the year, and the angular velocity gets higher and thus worse for observations with a rising elevation.

The same simulations have also been performed with the use of the focal reducer. In here, the same tendency for preferable directions is seen, but due to the larger field of view, more objects in total are detected. As result, again the simulation for the reference day is shown (Figure 8).

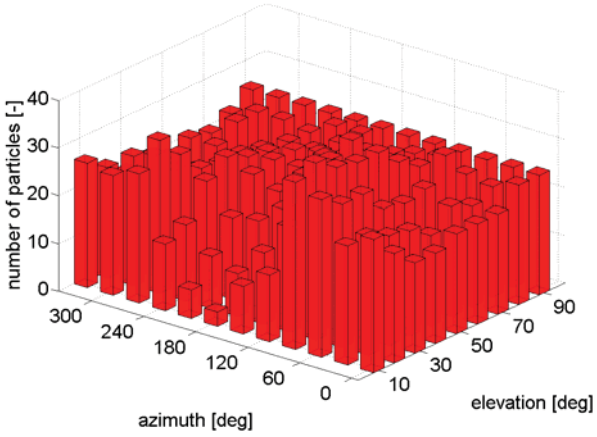

Figure 8: Number of particles per night, reference day, Andor camera with focal reducer. Peeks are observable for el = 10° and az = 90° and az = 270°.

It can be seen that the distribution of detected objects is very similar to those without the focal reducer. But as expected, the total amount of objects is much higher, approximately double as many. For an overview, the amounts of particles as well as the preferable direction on May 1st are given in TAB 4 and TAB 5. The values in brackets again account for simulations with the focal reducer, if different.

camera	max. number	min. number	mean
Andor	20.8 (37)	2.8 (3)	12.7 (23.6)
FLI	28 (50)	3 (6)	11.6 (24.2)
Perfect	57	5	36.5

TAB 4: minimum and maximum numbers of detected particles, reference day.

Camera	Azimuth [°]	Elevation [°]
Andor	90	10 (20)
FLI	90 (60)	10
Perfect	90	10

TAB 5: Preferable directions, reference day.

From the results of these simulations, one might furthermore deduct the impact of the viewing direction on the observation times for the objects. One can assume that changing the viewing direction in staring mode also changes the times, when the first or last particle is visible, due to the different illumination. Using this, one could extend the observation time by first looking east (when the sun has just set in west, and the east-sky is already dark) and then later turning into west, when the sun is too low to illuminate objects on the eastern sky. Figure 9 shows the results of an analysis of such an approach. It can be seen that the viewing direction does not clearly extend the observation time for the simulation conditions in any detectable way. This is reasoned by the very little section of the night sky observable from one site. Due to this, the times of first and last light on objects change only a little. The small amount of particles further amplifies the impact of this effect. The results depicted below are valid for the perfect camera, the other cameras yield a very similar output, just are not as smooth due to less detected objects and thus a lower statistical significance.

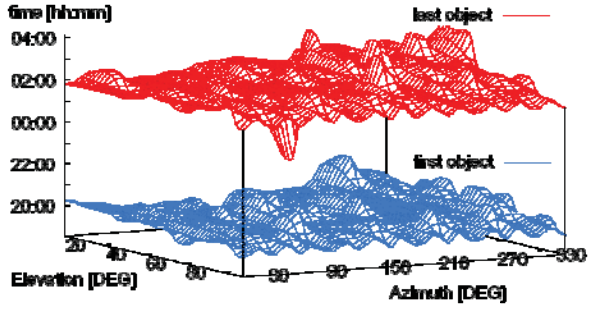

Figure 9: Detection clock times for perfect camera.

4.3.3. Long term simulations

Another critical point for a space debris surveillance station is the total number of objects and also the number of new and different objects that can be seen throughout a long observation time. For this, for all cameras, long term simulations have been performed. Long term refers at this point to simulations lasting one month, while staring into the prior determined preferred direction. Again, the simulations have been performed for different times during the year, February, May, August and November. TAB 6 shows the results for the reference day.

	Andor	FLI	perfect
Detected objects	649	682	1997
Different objects	616	567	1882
Fragments	76	38	490
NaK-Droplets	36	0	738
SRM	0	0	2
TLE-Objects	488	513	606
Westford-Needles	0	0	0
MLI	16	16	46

TAB 6: Detected objects during long term observations, Reference day.

In here, again the advantage of a large field of view can be seen, as the FLI camera detects slightly more objects than the Andor camera. But when looking on new objects only (i.e. objects that are non TLE objects), due to its better sensitivity, the Andor camera gains better results. When breaking this down to single observation periods, which are typically one nightfall or one daybreak, one gets roughly 10 objects per campaign or about 5 objects per hour with the Andor camera. Currently an improvement of these results by combining different sites is under investigation.

5. SPACE DEBRIS LASER RANGING

Once, when tracking sun illuminated space debris objects with suitable focal plane arrays as explained before is well established, it will be desired to follow up a range measurement with an aligned laser ranging system. This additional measurement will improve the calculated orbit considerably. A DLR concept was presented in 2011[5] and experimentally proved in early 2012 in collaboration with the SLR station in Graz[3]. During the campaign several meter class space debris objects for instance rocket bodies were tracked passively and ranged actively afterwards. The results will be published in this year.

5.1. Link budget calculation

To estimate the future requirements for a space debris laser ranging system we calculate the relation between laser pulse energy and space debris diameter for a typical kHz laser ranging station. Recent results from dedicated SLR station are used to evaluate the calculations. Therefore the offset of the curve was determined using the parameters of the Graz SLR station: receiver aperture of

[3] www.ifw.oeaw.ac.at/de/forschung/erdkoerper/slr-technologie/slr-station-graz-lustbuehel/

0.5 m; FoV of 40 arcsec; laser transmitter aperture of 0.1 m, beam spread of 7 arcsec, total transmission coefficient of 0.3, return rate of 0.01. For the measurement campaign DLR provided a 25 mJ laser system with a repetition rate of 1 kHz at a wavelength of 532 nm. Therefore it was possible to use statistical methods to select tracks during the short flyby period. These experimental results demonstrate for the first time the feasibility to track space debris objects with a low energy but high repetition rate laser ranging system. SLR stations using Joule class laser systems with low repetition rates also published tracks[6] of ranged meter class objects.

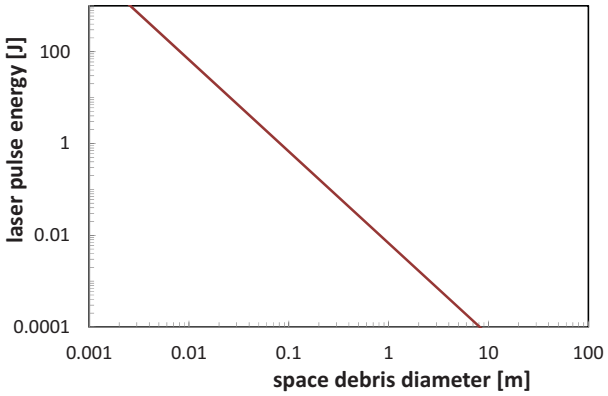

BILD 1. Figure 10: Required laser pulse energy to range space debris with specific diameter for a typical kHz SLR station.

In Figure 10 the estimated laser pulse energy to range smaller space debris objects is shown. Currently two different laser technologies are available. First, the kHz range low energy (25 mJ) pulse laser as used during the Graz campaign. On the opposite a few 1-2 joule laser systems which are installed on SLR station Mount Stromlo, Shanghai[5] and Grasse limited by their repetition rate of 10-50 Hz. The advantage of high repetition rate SLR stations is the possibility to use statistical analyses tools with very low return rates. Comparing the results of both technologies there is currently no distinguished advantage due to the operation of high energy laser pulses.

At DLR Institute for Technical Physics in Stuttgart a dedicated laser system is under development. This laser system is especially designed for laser-ranging sub-meter class space debris objects. The goal is to achieve a joule class laser system with more than 1 kHz repetition rate in the near infrared spectral band. Additional laser features will be included to fulfill the unique requirements in space situational awareness environment. It is expected to push the range measurement into the 10 cm region.

6. CONCLUSION

In this paper it was shown that it will be possible to acquire and detect space debris objects with the hardware available for the DLR passive optical test station at Stuttgart Uhlandshöhe. Next step will be the evaluation of the analytical calculations and PROOF simulation during experiments and measurement campaign on-site. Future estimated orbit determinations provide hand over data for a secondary laser-transmitter and ranging station. It was pointed out that the general acquisition of orbiting objects with laser ranging was shown to be possible, and the requirements for a laser to improve this process to detect smaller objects than to this point where given.

[1] Coates, C., Fowler, B., & Holst, G. (2009, June 06). A High-Performance Imaging Breakthrough.

[2] Daniels, G. M. (1977). A Night Sky Model for Satellite Search Systems. *Journal of Optical Engineering, Vol. 16, No. 1*, pp. 66-71.

[3] Gelhaus, J., Flegel, S., & Wiedemann, C. (2011). *Program for Radar and Optical Observation Forecasting: Final Report.* Braunschweig: Institut für Luft- und Raumfahrtsysteme, Technische Universität Braunschweig.

[4] Plane Wave Instruments. (2012). *17 inch CDK Optical Tube Assembly*. Retrieved 08/20/2012, from http://www.planewave.com

[5] Voelker, U., Buske, I., Riede, W., Speiser, J., & Giesen, A. (2011). Laser-Based Space Debris Monitoring at DLR.

[6] Zhang, Z.-P., Yang, F.-M., Zhan, H.-F., Wu, Z.-B., Chen, J.-P., Li, P., et al. (2012). The use of laser ranging to measure space debris. *Research in Astronomy and Astrophysics, Vol. 12 No.2*, pp. 212-218.